MODELLING THERMAL DEFORMATIONS IN CURVED COMPOSITE LAMINATES USING STANDARD SHELL FINITE ELEMENTS

Enrique Graciani[1], Antonio Blázquez[1], Jesús Justo[1] and Federico París[1]

[1]Grupo de Elasticidad y Resistencia de Materiales, Escuela Técnica Superior de Ingeniería, Universidad de Sevilla, c/Camino de los Descubrimientos s/n, 41092, Sevilla, Spain
[1]Email: egraciani@us.es, abg@us.es, jjusto@us.es, fparis@us.es, Web Page: http://www. us.es

Keywords: Finite elements, thermal deformations, spring-in, shells

Abstract.
A novel technique for predicting thermal deformations of components made of composite laminates using finite element models with standard shell elements is introduced. To take into account the effect of the coefficient of thermal expansion in the through-thickness direction and the curvature of the laminate, appropriate fictitious coefficient of thermal expansions are defined in the in-plane directions. To validate the new modelling approach, numerical results have been successfully compared with 3D finite element models, showing an excellent agreement.

1. Introduction

One of the main drawbacks in the use of composites for manufacturing large structural components is the difficulty in achieving acceptable tolerances in the final size and shape of the components.

In a classical autoclave manufacturing process, the final shape of the manufactured component depends on the chemical shrinkage of the material during solidification, the adhesion between the mould and the component and the thermal shrinkage during cooling after solidification. Most of these phenomena are difficult to characterize and present orthotropic behaviour in each layer of the laminate, thus being very challenging to accurately predict the final shape of the part from the nominal dimensions of the moulds and the lay-ups employed for the component.

In this paper a novel technique for predicting thermal deformations of components made of composite laminates using finite element (FE) models is introduced. Although the determination of thermal expansions with finite elements is a well-stablished problem, deeply studied in the literature, its application to large composite laminate has inherent difficulties that make FE analysis very expensive. The main characteristic is that thermal deformations are associated to the different values of the coefficients of thermal expansion (CTE) in the orthotropic directions of the composite laminas. For that reason, deformation of curved parts is significantly affected by the CTE in the through-thickness direction, making necessary the use of 3D elements or special shell elements for modelling the problem [1].

The novel technique introduced in this paper permits the FE modelling of thermal deformations in curved laminates using standard shell elements by defining appropriately fictitious in-plane CTE of the material to take into account the effect of the curvature of the laminate represented by the shell element. To show the accuracy of the method a simple L-shape sample is employed and results obtained with the shell FE models are compared with results obtained with solid FE models.

Excerpt from ISBN 978-3-00-053387-7

The procedure for defining the fictitious in-plane CTE is described, firstly, for curved homogeneous orthotropic materials (with the orthotropic directions not necessarily being parallel to the L sides) and, secondly, for curved composite laminates. In all cases, results obtained with the shell FE models show an excellent agreement with results obtained with the solid FE models.

2. Problem

The geometry of the problem considered is shown in Figure 1(a). A L-shaped composite sample of width $W = 16$ mm is employed. The length of the flat wings is $L = 16$ mm, the mean radius of the curved part is $R = 3.8$ mm and the thickness is $t = 1.6$ mm. Initially the angle formed by the L wings is $\beta = 90°$. After cooling, the differences between the through-thickness and the in-plane CTE makes this angle to become smaller, phenomenon typically referred as springback or spring-in [2]. Samples have been clamped at the extreme of the horizontal wing. Only symmetric laminates are considered, therefore the flat parts of the sample remain practically flat after cooling. Thus, the spring-in angle $\Delta\beta$ is defined from the displacements of the vertical wing in the direction normal to its plane; see Figure 1(b).

Four different lay-ups have been considered: two configurations, $[0_8]$ and $[90_8]$, correspond to homogeneous materials with in-plane orthotropic directions parallel to the L sides, the third configuration, $[-45_8]$, is also homogeneous but the in-plane orthotropic directions are not parallel to the L sides and, finally the fourth configuration, $[0,90,+45,-45]_S$, is a laminate with differently oriented layers.

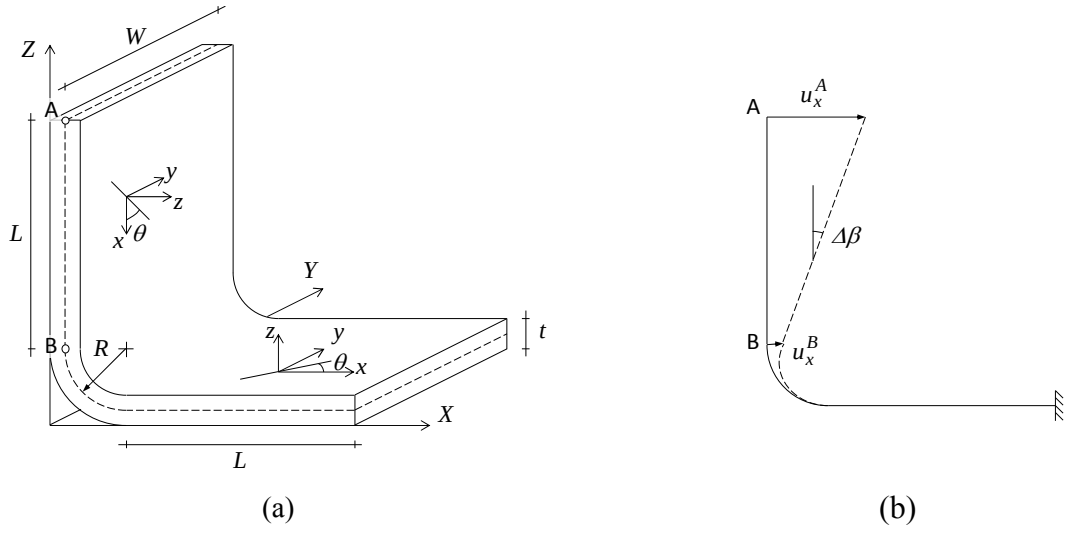

Figure 1. (a) Geometry and dimensions of the problem; (b) boundary conditions and definition of the spring-in angle $\Delta\beta$.

Mechanical properties of the layers are defined by: $E_{11} = 125$ GPa, $E_{22} = E_{33} = 10$ GPa (with 1 being the fibre direction, 2 being the in-plane direction perpendicular to the fibre and 3 the through-thickness direction), $G_{12} = G_{23} = G_{31} = 4$ GPa, $\nu_{12} = \nu_{13} = 0.3$, $\nu_{23} = (E_{33}/2G_{23}) - 1 = 0.25$. The so-called small Poisson ratio is $\nu_{21} = \nu_{31} = \nu_{13}E_{33}/E_{11} = 0.024$. Orthotropic CTE of the laminas are: $\alpha_1 = -1 \cdot 10^{-6}\ \mathrm{K}^{-1}$, $\alpha_2 = 25 \cdot 10^{-6}\ \mathrm{K}^{-1}$, $\alpha_3 = 50 \cdot 10^{-6}\ \mathrm{K}^{-1}$. A cooling of $\Delta T = -155$ K is imposed.

Excerpt from ISBN 978-3-00-053387-7

FE models are created using standard MSC.Nastran solid and shell elements with appropriate material properties (fictitious in some cases) as detailed in the following section. As shown in Figure 2(a), solid FE mesh has only one element per layer in the thickness direction, and the size of in-plane element sides are double than the through-thickness side to keep a good aspect ratio in the element. In the shell model element size in the straight direction is identical to the one employed in the solid mesh and along the curved zone double number of shell elements are employed in comparison to one layer of the solid model. Although not shown here for the sake of brevity, once a reasonable size of the element is employed results are insensitive to the mesh size, the number of elements needed to obtain a reasonable accuracy being much smaller when shell elements are employed.

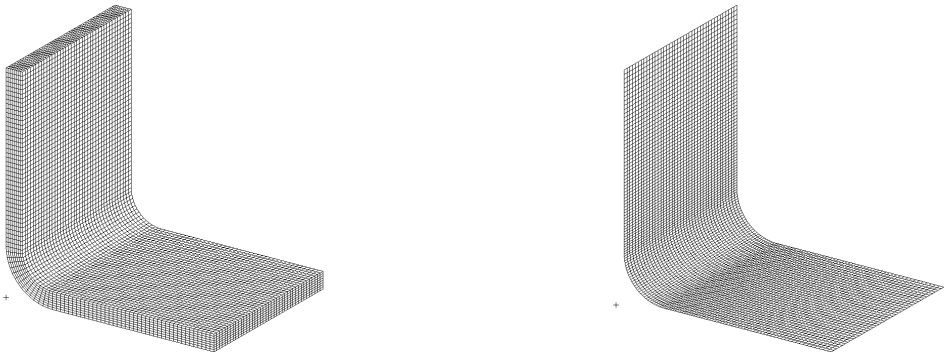

(a) (b)

Figure 2. (a) Solid FE mesh; (b) shell FE mesh.

3. Definition of material properties in the solid models

Solid FE model are made of MSC.Nastran 8-nodes hexahedral element CHEXA. A uniform mesh of solid elements has been used where the y direction of the element's co-ordinate system is always parallel to the global Y direction shown in Figure 1(a), the z direction of the element's co-ordinate system is the through-thickness direction and the x direction of the element's co-ordinate system is perpendicular to both. As can be seen in Figure 1(a), the orthotropic directions of the material are different in the vertical and the horizontal wings of the L sample, and consequently vary along the curved zone of the model. To define material properties easily, the material's coordinate system is identified with the element's coordinate system, using a PSOLID entry. In the element's coordinate system, all elements in each layer have the same material properties. If the fibre direction forms an angle θ with the x direction of the element's co-ordinate system, orthotropic material properties defined in the previous section have to be rotated to obtain the material constants. For the sake of clarity (and to avoid confusion since no standard notation is employed in the literature) the procedure employed for the rotation of the orthotropic properties to obtain the apparent anisotropic properties in the element's coordinate system is described in the following.

Constitutive equation in the orthotropic co-ordinate system of each layer is given by:

$$\begin{aligned} &\boldsymbol{\sigma}_O^{3D} = \mathbf{Q}_O^{3D}[\boldsymbol{\varepsilon}_O^{3D} - \boldsymbol{\varepsilon}_O^{T,3D}] \ , \ \boldsymbol{\sigma}_O^{3D} = [\sigma_{11} \quad \sigma_{22} \quad \sigma_{33} \quad \sigma_{12} \quad \sigma_{23} \quad \sigma_{31}]^T \ , \\ &\boldsymbol{\varepsilon}_O^{3D} = [\varepsilon_{11} \quad \varepsilon_{22} \quad \varepsilon_{33} \quad \gamma_{12} \quad \gamma_{23} \quad \gamma_{31}]^T \ , \ \boldsymbol{\varepsilon}_O^{T,3D} = [\alpha_1 \Delta T \quad \alpha_2 \Delta T \quad \alpha_3 \Delta T \quad 0 \quad 0 \quad 0]^T \end{aligned} \tag{1}$$

Excerpt from ISBN 978-3-00-053387-7

where σ_{ij} and ε_{ij}, with $i,j=1,2,3$, are the components of the stresses and strains in the orthotropic co-ordinate system of each layer. The components of the stiffness matrix $\boldsymbol{Q}_O^{3D}$ are given in the Appendix.

Constitutive equation in element's co-ordinate system in each layer is obtained rotating (1):

$$\begin{gathered}\boldsymbol{\sigma}_E^{3D}=\boldsymbol{Q}_E^{3D}[\boldsymbol{\varepsilon}_E^{3D}-\boldsymbol{\varepsilon}_E^{T,3D}]\ ,\ \boldsymbol{\sigma}_E^{3D}=[\sigma_{xx}\quad\sigma_{yy}\quad\sigma_{zz}\quad\sigma_{xy}\quad\sigma_{yz}\quad\sigma_{zx}]^T=[L^{3D}]^{-1}\boldsymbol{\sigma}_O^{3D}\ ,\\ \boldsymbol{\varepsilon}_E^{3D}=[\varepsilon_{xx}\quad\varepsilon_{yy}\quad\varepsilon_{zz}\quad\gamma_{xy}\quad\gamma_{yz}\quad\gamma_{zx}]^T=\boldsymbol{R}^{3D}[\boldsymbol{L}^{3D}]^{-1}[\boldsymbol{R}^{3D}]^{-1}\boldsymbol{\varepsilon}_O^{3D}\ ,\\ \boldsymbol{\varepsilon}_E^{T,3D}=[\alpha_{xx}\Delta T\quad\alpha_{yy}\Delta T\quad\alpha_{zz}\Delta T\quad\alpha_{xy}\Delta T\quad 0\quad 0]^T=\boldsymbol{R}^{3D}[\boldsymbol{L}^{3D}]^{-1}[\boldsymbol{R}^{3D}]^{-1}\boldsymbol{\varepsilon}_O^{T,3D}\end{gathered}\tag{2}$$

where σ_{ij} and ε_{ij}, with $i,j=x,y,z$, are the components of the stresses and strains in the element's co-ordinate system. The stiffness matrix $\boldsymbol{Q}_E^{3D}$ and the auxiliary matrices $\boldsymbol{L}^{3D}$ and $\boldsymbol{R}^{3D}$ used for the rotation are given in the Appendix.

4. Definition of material properties in the shell models

Shell FE model are made of MSC.Nastran 4-nodes quadrilateral element CQUAD4. Shell element's coordinate system is oriented as described for the solid element's coordinate system. To define material properties easily, the material's coordinate system in all layers is identified with the element's coordinate system, using a PCOMP entry. Therefore, in the layers where the fibre direction forms an angle θ with the x direction of the element's co-ordinate system, orthotropic material properties have to be rotated to obtain the material constants. In the following it is described, first, the procedure employed for the rotation of the orthotropic properties to obtain the apparent anisotropic properties in the element's coordinate system and, second, the procedure employed to define the fictitious CTE to take into account the curvature of the laminate in the x direction of the element's co-ordinate system.

Plane stress constitutive equation in orthotropic co-ordinate system of each layer is given by:

$$\begin{gathered}\boldsymbol{\sigma}_O^k=\boldsymbol{Q}_O^k[\boldsymbol{\varepsilon}_O^k-\boldsymbol{\varepsilon}_O^{T,k}]\ ,\ \boldsymbol{\sigma}_O^k=[\sigma_{11}^k\quad\sigma_{22}^k\quad\sigma_{12}^k]^T\ ,\ \boldsymbol{\varepsilon}_O^{kk}=[\varepsilon_{11}^k\quad\varepsilon_{22}^k\quad\gamma_{12}^k]^T\ ,\\ \boldsymbol{\varepsilon}_O^{T,k}=[\alpha_1^k\Delta T\quad\alpha_2^k\Delta T\quad 0]^T\ ,\end{gathered}\tag{3}$$

where σ_{ij}^k and ε_{ij}^k, with $i,j=1,2$, are the in-plane components of the stresses and strains in the orthotropic co-ordinate system of layer k, with $k=1$ being the outer layer (i.e., the layer placed in the largest radius) and $k=8$ being the inner layer. The components of the stiffness matrix $\boldsymbol{Q}_O^k$ are given in the Appendix. In the plane zones of the model, $\alpha_i^k=\alpha_i$, with $i=1,2$. Definition of CTE in the curved zone is not straightforward and will be treated in a separate section below. Plane stress constitutive equation of each layer in element's co-ordinate system is obtained rotating (3):

$$\begin{gathered}\boldsymbol{\sigma}_E^k=\boldsymbol{Q}_E^k[\boldsymbol{\varepsilon}_E^k-\boldsymbol{\varepsilon}_E^{T,k}]\ ,\ \boldsymbol{\sigma}_E^k=[\sigma_{xx}^k\quad\sigma_{yy}^k\quad\sigma_{xy}^k]^T=[L^k]^{-1}\boldsymbol{\sigma}_O^k\ ,\\ \boldsymbol{\varepsilon}_E^k=[\varepsilon_{xx}^k\quad\varepsilon_{yy}^k\quad\gamma_{xy}^k]^T=\boldsymbol{R}^{2D}[\boldsymbol{L}^k]^{-1}[\boldsymbol{R}^{2D}]^{-1}\boldsymbol{\varepsilon}_O^k\ ,\\ \boldsymbol{\varepsilon}_E^{T,k}=[\alpha_{xx}^k\Delta T\quad\alpha_{yy}^k\Delta T\quad\alpha_{xy}^k\Delta T]^T=\boldsymbol{R}^{2D}[\boldsymbol{L}^k]^{-1}[\boldsymbol{R}^{2D}]^{-1}\boldsymbol{\varepsilon}_O^{T,k}\ ,\end{gathered}\tag{4}$$

Excerpt from ISBN 978-3-00-053387-7

where σ_{ij}^k and ε_{ij}^k, with $i,j=x,y$, are the in-plane components of the stresses and strains in the element's co-ordinate system. The stiffness matrix $\boldsymbol{Q}_E^k$ and the auxiliary matrices $\boldsymbol{L}^k$ and $\boldsymbol{R}^{2D}$ used for the rotation are given in the Appendix. Stiffness constants and CTE in the plane zones of the model depend only on the orientation of the layer and are summarized in Table 1.

Table 1. Stiffness constants and CTE in the plane zones of the model, in element's coordinate system.

Orientation	$\overline{Q}_{11}^k$	$\overline{Q}_{12}^k$	$\overline{Q}_{13}^k$	$\overline{Q}_{22}^k$	$\overline{Q}_{32}^k$	$\overline{Q}_{33}^k$	α_{xx}^k	α_{yy}^k	α_{xy}^k
(°)	(GPa)						(10^{-6}K^{-1})		
0	125.9	3.022	0	10.07	0	4	−1	25	0
90	10.07	3.022	0	125.9	0	4	25	−1	0
±45	39.51	31.51	∓28.96	39.51	∓28.96	32.48	−12	−12	±26

The procedure used to define the fictitious CTE to take into account the curvature of the laminate in the x direction of the element's co-ordinate system in the homogeneous samples, $[0_8]$, $[90_8]$ and $[-45_8]$, is different from the procedure used in the inhomogeneous sample $[0,90,+45,-45]_S$. These two cases are treated separately in the following sections.

4.1. Homogeneous samples

One of the difficulties in employing shell elements is that its formulation does not take into account the material shrinkage in the through-thickness direction. To overcome this problem, the thermal strains of the actual material are considered as a superposition of the thermal strains of two fictitious materials. One, named material B, having all CTE equal to α_3 and the other, named material A, having CTE equal to $\alpha_i-\alpha_3$, with $i=1,2,3$. In this manner, when the sample of material B is subjected to an uniform temperature change it will suffer a change in size without change in shape. On the contrary, the sample of material A will suffer identical change in shape than the sample of the original material, (although different change in size). Therefore, the in-plane CTE in each layer of materials A and B are initially given by:

$$\alpha_1^{A,k}=\alpha_1-\alpha_3\ ,\ \ \alpha_2^{A,k}=\alpha_2-\alpha_3\ ,\ \ \alpha_1^{B,k}=\alpha_3\ ,\ \ \alpha_2^{B,k}=\alpha_3 \tag{5}$$

The second difficulty in employing shell elements is that each layer k of the shell has a different length, since is located at a different radial position $r_k=R+\frac{1}{16}(2k-7)t$, with $k=1,...,8$. Since the formulation of classical shell elements does not consider that each layer may have a different length, all layers have identical thermal elongations, thus not reproducing the change in shape of the actual material. To overcome this problem, CTE of material A along the curved direction x is modified to take into account the different length of each layer:

$$\hat{\alpha}_{xx}^{A,k}=\frac{r_k}{R}\alpha_{xx}^{A,k} \tag{6}$$

Finally, fictitious CTE along the curved direction x in each layer is obtained as the sum of the fictitious CTE of material A, $\hat{\alpha}_{xx}^{A,k}$, and the CTE of material B, $\alpha_{xx}^{B,k}$:

Excerpt from ISBN 978-3-00-053387-7

$$\alpha_{xx}^{k} = \hat{\alpha}_{xx}^{A,k} + \alpha_{xx}^{B,k} = \frac{r_k}{R}\alpha_{xx}^{A,k} + \alpha_{xx}^{B,k},\ \alpha_{yy}^{k} = \alpha_{yy}^{A,k} + \alpha_{yy}^{B,k},\ \alpha_{xy}^{k} = \alpha_{xy}^{A,k} + \alpha_{xy}^{B,k}. \quad (7)$$

Fictitious CTE along the curved direction x in each layer are summarized in Table 2. The remaining in-plane CTE are not affected by the procedure described above, therefore are identical to those listed in Table 1.

Table 2. Fictitious CTE along the curved direction x in each layer of the homogeneous samples.

Orientation	$\alpha_{xx}^{A,k}$	α_{xx}^{1}	α_{xx}^{2}	α_{xx}^{3}	α_{xx}^{4}	α_{xx}^{5}	α_{xx}^{6}	α_{xx}^{7}	α_{xx}^{8}
(°)	(10^{-6}K^{-1})	(10^{-6}K^{-1})							
0	–51	–10.4	–7.71	–5.03	–2.34	0.34	3.03	5.71	8.39
90	–25	20.4	21.7	23.0	24.3	25.7	27.0	28.3	29.6
±45	–38	5	7	9	11	13	15	17	19

4.2. Laminates

The procedure described above for a homogeneous material is based on the fact that, in that case, the spring-in angle, $\Delta\beta$, can be easily calculated as $\Delta\beta = (\alpha_{xx} - \alpha_{zz})\Delta T\beta$. In composite laminates, analytical calculation of the spring-in angle can also be determined, although the presence of residual stresses makes the calculations more complicated [3]. Therefore, once the spring-in angle $\Delta\beta$ is known, an equivalent CTE along the curved direction x can be obtained as:

$$\overline{\alpha}_{xx} = \frac{\Delta\beta}{\Delta T\beta} + \alpha_{zz}. \quad (8)$$

This equivalent CTE can be modified to take into account the different length of each layer, resulting in the following fictitious CTE for each layer of the laminate along the curved direction x:

$$\alpha_{xx}^{k} = \frac{r_k}{R}(\overline{\alpha}_{xx} - \alpha_{zz}) + \alpha_{zz}. \quad (9)$$

Fictitious CTE along the curved direction x in each layer of the $[0,90,+45,-45]_S$ sample are summarized in Table 3. The stiffness properties and the remaining in-plane CTE are not affected by the procedure described above. Therefore these properties are defined, in each layer, by the values shown in Table 1.

Table 3. Fictitious CTE along the curved direction x in each layer of the composite laminate sample.

(°)	(10^{-6}K^{-1})	(10^{-6}K^{-1})							
$\Delta\beta$	$\overline{\alpha}_{xx}$	α_{xx}^{1}	α_{xx}^{2}	α_{xx}^{3}	α_{xx}^{4}	α_{xx}^{5}	α_{xx}^{6}	α_{xx}^{7}	α_{xx}^{8}
0.749	–3.68	6.20	3.38	0.55	–2.27	–5.10	–7.92	–10.7	–13.6

Excerpt from ISBN 978-3-00-053387-7

5. Results

Spring-in angle $\Delta\beta$ obtained with the solid and shell FEM models in all samples are listed in Table 4. As can be seen, the agreement between the results of both modes is excellent in all cases. To show the ability of the shell model to reproduce appropriately the in-plane deformations, as well as the out-of-plane distortions, the solution of all components of the displacements along the edge AB depicted in Figure 1 is shown in Figure 3, for the $[90_8]$ sample and the $[0,90,+45,-45]_S$ sample.

Table 4. Results obtained for the spring-in angle in all samples considered.

	$\Delta\beta$ (°) [% difference]			
Model	$[0_8]$	$[90_8]$	$[-45_8]$	$[0,90,-45,+45]_S$
solid	0.711	0.348	0.522	0.744
shell	0.712	0.343	0.494	0.734

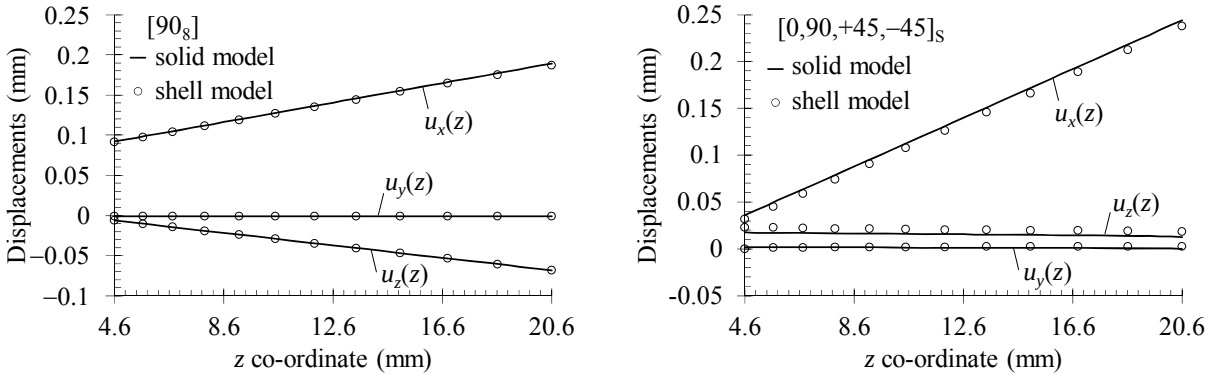

Figure 3. Displacements along the edge AB: (a) $[90_8]$ sample; (b) $[0,90,+45,-45]_S$ sample.

6. Conclusions

A new modelling procedure which enables the prediction of the spring-in for L-shaped composite samples with different stacking sequence using standard shell finite elements (with suitably modified coefficients of thermal expansion in the in-plane directions) is presented. To validate the new modelling approach, numerical results have been successfully compared with 3D finite element models, showing an excellent agreement. The new modelling procedure has a great potential for improving the efficiency in the model of more complicated geometries.

Appendix A. Stiffness and rotation matrices

Components of $\boldsymbol{Q}_O^{3D}$ are Q_{ij} with $i,j=1,...,6$. Non-null components are given by:

$$Q_{11}=\frac{E_{11}(1-\nu_{32}\nu_{23})}{\Delta}\ ,\ Q_{12}=Q_{21}=\frac{E_{22}(\nu_{12}+\nu_{32}\nu_{13})}{\Delta}\ ,\ Q_{13}=Q_{31}=\frac{E_{33}(\nu_{13}+\nu_{12}\nu_{32})}{\Delta}\ ,$$
$$Q_{22}=\frac{E_{22}(1-\nu_{13}\nu_{31})}{\Delta}\ ,\ Q_{33}=\frac{E_{33}(1-\nu_{12}\nu_{21})}{\Delta}\ ,\ Q_{23}=Q_{32}=\frac{E_{33}(\nu_{23}+\nu_{21}\nu_{13})}{\Delta}\ , \tag{10}$$
$$Q_{44}=G_{12}\ ,\ Q_{55}=G_{23}\ ,\ Q_{66}=G_{31}\ ,\ \Delta=1-\nu_{12}\nu_{21}-\nu_{23}\nu_{32}-\nu_{31}\nu_{13}-2\nu_{12}\nu_{23}\nu_{31}\,.$$

Excerpt from ISBN 978-3-00-053387-7

Components of $\boldsymbol{Q}_O^k$ are Q_{ij}^k with $i, j = 1,...,3$. Non-null components are given by:

$$Q_{11}^k = \frac{E_{11}}{1-\nu_{12}\nu_{21}} \ , \ Q_{22}^k = \frac{E_{22}}{1-\nu_{12}\nu_{21}} \ , \ Q_{12}^k = \frac{\nu_{12}E_{22}}{1-\nu_{12}\nu_{21}} \ , \ Q_{33} = G_{12} \ . \tag{11}$$

Matrx $\boldsymbol{Q}_E^{3D}$ and $\boldsymbol{Q}_E^k$ are given by:

$$\boldsymbol{Q}_E^{3D} = [\boldsymbol{L}^{3D}]^{-1}\boldsymbol{Q}_O^{3D}\boldsymbol{R}^{3D}[\boldsymbol{L}^{3D}][\boldsymbol{R}^{3D}]^{-1} \ , \ \boldsymbol{Q}_E^k = [\boldsymbol{L}^k]^{-1}\boldsymbol{Q}_O^k\boldsymbol{R}^{2D}[\boldsymbol{L}^k][\boldsymbol{R}^{2D}]^{-1} \ , \tag{12}$$

where rotation matrices $\boldsymbol{L}^{3D}$ and $\boldsymbol{L}^k$ are:

$$\boldsymbol{L}^{3D} = \begin{bmatrix} c^2 & s^2 & 0 & 2cs & 0 & 0 \\ s^2 & c^2 & 0 & -2cs & 0 & 0 \\ 0 & 0 & 1 & 0 & 0 & 0 \\ -cs & cs & 0 & c^2-s^2 & 0 & 0 \\ 0 & 0 & 0 & 0 & c & -s \\ 0 & 0 & 0 & 0 & s & c \end{bmatrix} \ , \ \boldsymbol{L}^k = \begin{bmatrix} c_k^2 & s_k^2 & 2c_k s_k \\ s_k^2 & c_k^2 & -2c_k s_k \\ -c_k s_k & c_k s_k & c_k^2 - s_k^2 \end{bmatrix}, \tag{13}$$

with $c = \cos\theta$, $s = \sin\theta$, $c_k = \cos\theta_k$ and $s_k = \sin\theta_k$. Auxiliary matrices $\boldsymbol{R}^{3D}$ and $\boldsymbol{R}^{2D}$ are needed to transform the engineering shear strains ($\gamma_{ij} = 2\varepsilon_{ij}$, with $i \neq j$). Therefore, no-diagonal terms of $\boldsymbol{R}^{3D}$ and $\boldsymbol{R}^{2D}$ are null, while diagonal terms are equal to 1 in the columns corresponding to the normal strains and equal to 2 in the columns corresponding to the shear strains.

Acknowledgments

This work has been partially supported by the Spanish Government (Ministerio de Economía y Competitividad, proyecto MAT2015-71309-P).

References

[1] H.W. Wiersma, L.J.B. Peeters, R and Akkerman. Prediction of springforward in continuous-fibre/ polymer L-shaped parts, *Composites Part A: Applied Science and Manufacturing*, 29:1333-1342, 1998.

[2] E. Kappel, D. Stefaniak and C. Hühne. Process distortions in prepreg manufacturing – An experimental study on CFRP L-profiles. *Composite Structures,* 106:615–625, 2013.

[3] A.J.M. Spencer, P. Watson and T.G. Rogers. Mathematical analysis of the springback effect in laminated thermoplastic channel sections. *Composites Manufacturing*, 2:253-258, 1991.

Excerpt from ISBN 978-3-00-053387-7